

ROVERFLY: Robust and Versatile Learning-based Control of Quadrotor Across Payload Configurations

Mintae Kim[†], Jiaze Cai, and Koushil Sreenath

Abstract—Designing robust controllers for precise, arbitrary trajectory tracking with quadrotors is challenging due to nonlinear dynamics and underactuation, and becomes harder with flexible cable-suspended payloads that introduce extra degrees of freedom and hybridness. Classical model-based methods offer stability guarantees but require extensive tuning and often do not adapt when the configuration changes—when a payload is added or removed, or when the payload mass or cable length varies. We present ROVERFLY, a unified learning-based control framework in which a reinforcement learning (RL) policy serves as a robust and versatile tracking controller for standard quadrotors and for cable-suspended payload systems across a range of configurations. Trained with task and domain randomization, the controller is resilient to disturbances and varying dynamics. It achieves strong zero-shot generalization across payload settings—including no payload as well as varying mass and cable length—without controller switching or re-tuning, while retaining the interpretability and structure of a feedback tracking controller. Code and supplementary materials are available at <https://github.com/mintaeshkim/roverfly>.

I. INTRODUCTION

Quadrotors are widely used for aerial navigation, and numerous planning and control strategies have been developed for agile and precise maneuvering [1], [2]. For payload transport, rigid (active) attachment increases manipulation capability but reduces agility due to higher inertia [3], whereas cable suspension preserves maneuverability and enables multi-UAV cooperation at the cost of additional underactuation and nonlinear dynamics [4], [5].

Prior work on quadrotor-payload systems falls into three directions: (1) generating and tracking payload trajectories that suppress swing [6], [7], [8]; (2) controlling systems with elastic/flexible cables and pulley mechanisms [9], [10], [11]; and (3) cooperative manipulation with multiple quadrotors [7], [10]. Most approaches use model-based geometric control leveraging differential flatness [4], [12]. While these methods offer theoretical guarantees, they require accurate models and extensive tuning, and often do not generalize to dynamic or uncertain settings. A key limitation is the need for separate controller designs for different configurations (with vs. without payload) [1], [13], which necessitates controller switching in practice and can introduce instability. Moreover, reliance on flatness requires precomputed trajectories and precludes tracking dynamically infeasible references.

Model-free RL has emerged as a promising paradigm for UAV control, learning feedback policies directly from inter-

action without explicit dynamics modeling [2], [14], [15], [16]. This is particularly compelling for UAVs, whose high-rate, nonlinear, underactuated, and aerodynamically coupled dynamics are difficult to model and tune accurately [17], [18]. RL controllers have shown robust trajectory tracking [19], cross-platform adaptation [20], disturbance rejection [21], and the ability to track dynamically infeasible trajectories [15]. However, neither existing RL nor model-based methods adequately handle rapidly varying payload conditions such as changes in mass or cable length, and there is no RL controller explicitly designed for flexible cable-suspended payload tracking.

Table I summarizes the landscape. Racing-oriented learning controllers excel on fixed courses with specialized perception/estimation stacks but are not intended for arbitrary references or payload handling [2]. General-purpose RL benchmarking suites enable reproducible studies yet encourage task-specific rewards and typically train a separate policy per task rather than a single versatile controller [22]. Hybrid learning-plus-adaptive control can follow references and reject wind but relies on a nominal model and an additional adaptive layer, with demonstrations mainly on relatively simple, planar motions [15]. Methods that adapt via latent extrinsics capture cross-platform variation near hover but require an adaptation phase and are evaluated chiefly under small-impulse disturbances [20]. Taken together, these limitations point to the need for a controller that tracks arbitrary references while accommodating unknown payload presence, cable length, and mass—without per-task policies or controller switching.

We introduce a learning-based tracking controller that operates across varying payload and cable configurations—using a *single* policy with no switching or re-tuning. Task and domain randomization make the policy robust to underactuation, nonlinear dynamics, changing task conditions, and disturbances. Drawing on hybrid dynamics and POMDP insights, we use I/O history as a belief-state proxy so the policy acts as an implicit observer under partial observability. The result is a single RL-learned feedback law that unifies hovering, takeoff, landing, and arbitrary trajectory tracking while avoiding task-specific reward engineering or environment-specific tuning.

Contributions. (i) *Unified control framework*: a single policy for robust arbitrary trajectory tracking in both quadrotor-only and flexible cable-suspended payload systems, generalizing across payload mass and cable length without fine-tuning. (ii) *RL for flexible payload tracking*: an versatile RL-based controller explicitly targeting flexible cable-suspended pay-

[†] Corresponding author (e-mail: mintae.kim@berkeley.edu)

The authors are with *Hybrid Robotics Lab*, University of California, Berkeley, CA 94720, United States.

TABLE I: Comparison of learning-based quadrotor control approaches.

Criteria	[2]	[22]	[15]	[20]	ROVERFLY
Arbitrary trajectory tracking	\times	\times	\checkmark	\times	\checkmark
Robustness under disturbances	\times	\times	\checkmark	\triangle Small impulse	\checkmark
Versatility to varying tasks	–	\times	–	\triangle Hovering only	\checkmark
Adaptation to varying environments	\times	\times	\times	\checkmark	\checkmark
Agnostic to system dynamics	\checkmark	\checkmark	\times	\checkmark	\checkmark

loads with strong zero-shot performance via task and domain randomization. (iii) *Belief-based use of I/O history*: a justification for incorporating I/O history grounded in POMDP belief propagation and hybrid dynamics analysis, showing its role in reducing uncertainty and improving performance under partial observability.

II. RELATED WORK

A. Model-Based Control and Trajectory Planning for Quadrotor-Payload Systems

Model-based approaches—particularly geometric control—provide formulations with almost-global stability guarantees for quadrotor–payload systems [4], [6], [7], [12]. Via differential flatness, they plan trajectories by expressing states and inputs as flat outputs, ensuring feasibility. Geometric controllers on this principle track both quadrotor and payload trajectories [1], [4]. Recent work extends these methods to elastic or flexible cables [9], [10], introducing higher-order dynamics and greater underactuation. However, they require accurate models, frequent retuning, and are sensitive to unmodeled effects (e.g., actuator saturation, external disturbances), limiting robustness in practice.

Trajectory-generation methods likewise plan dynamically feasible payload motions. Optimization-based approaches such as mixed-integer quadratic programming (MIQP) [6] and mathematical programs with complementarity constraints (MPCC) [8] handle hybrid dynamics and cable-tension regimes for swing suppression and obstacle avoidance. MIQP is computationally heavy, while MPCC improves efficiency but remains model- and tuning-sensitive; as a result, these methods are typically used offline or in settings with limited real-time adaptability.

B. Learning-based Control of Quadrotors

Model-free RL has become a practical tool for quadrotor flight, enabling high-performance trajectory tracking and agile maneuvers without explicit system identification. In this view, the learned policy acts as a nonlinear feedback controller that adapts to complex dynamics from data. RL controllers show disturbance rejection when paired with adaptive elements [15], improved sample efficiency and sim-to-real transfer with recent training strategies [23], and race-level performance where simulation-trained controllers surpassed human pilots [2].

Despite this progress, payload trajectory tracking—especially with flexible, cable-suspended payloads—remains underexplored. One exception learns a dynamics model from human demonstrations and embeds

TABLE II: Notation and definitions for the quadrotor–payload system.

$m_Q \in \mathbb{R}$	Mass of the quadrotor
$\mathbf{J}_Q \in \mathbb{R}^{3 \times 3}$	Inertia matrix of the quadrotor w.r.t. the body-fixed frame
$\mathbf{R} \in SO(3)$	Rotation matrix from the body-fixed frame to the inertial frame
$\boldsymbol{\Omega} \in \mathbb{R}^3$	Angular velocity of the quadrotor in the body-fixed frame
$\mathbf{x}_Q, \mathbf{v}_Q \in \mathbb{R}^3$	Position and velocity of the quadrotor CoM in the inertial frame
$\mathbf{x}_Q^d, \mathbf{v}_Q^d \in \mathbb{R}^3$	Desired quadrotor position and velocity from the reference trajectory
$f \in \mathbb{R}$	Magnitude of the total thrust
$\mathbf{M} \in \mathbb{R}^3$	Body-frame moment
$\mathbf{w}_F \in \mathbb{R}^3$	External force disturbance on the system CoM
$\mathbf{w}_M \in \mathbb{R}^3$	External moment disturbance applied to the quadrotor
$m_P \in \mathbb{R}$	Mass of the suspended load
$\mathbf{q} \in S^2 \subset \mathbb{R}^3$	Unit vector from quadrotor to load (cable direction)
$\boldsymbol{\omega} \in \mathbb{R}^3$	Angular velocity of the suspended load
$\mathbf{x}_P, \mathbf{v}_P \in \mathbb{R}^3$	Position and velocity of the suspended load (inertial frame)
$\mathbf{x}_P^d, \mathbf{v}_P^d \in \mathbb{R}^3$	Desired payload position and velocity from the reference trajectory
$l \in \mathbb{R}$	Cable length
$T \in \mathbb{R}$	Cable tension magnitude
$\bar{f} \in \mathbb{R}$	Max total thrust
$\bar{\Omega} \in \mathbb{R}$	Max body rate
$\bar{M}, \underline{M} \in \mathbb{R}$	Max and min body-frame moment

it in MPC for stabilization [24], but targets near-static, vertically suspended loads, limiting dynamic maneuvering. Other high-performance results rely on precise estimation stacks and specialized hardware yet are restricted to fixed racing courses, limiting generalization [2]. Simulation frameworks offer task flexibility via modular rewards but typically require training a separate policy per task [22].

Robustness to hardware/parameter variation has been addressed by learning latent extrinsics such as mass or thrust [20], though these approaches require an adaptation phase and are mostly validated near hover. Hybrid RL with adaptive control improves robustness and can track arbitrary references, but still assumes partially known dynamics and is shown in constrained scenarios [15]. These gaps motivate a unified, general-purpose learning-based controller that serves as a single robust tracker across diverse quadrotor tasks—including payload manipulation—without task-specific design, controller switching, or retraining.

III. PROBLEM DESCRIPTION

A. System Dynamics

We consider two quadrotor variants: (1) a standard platform, and (2) a quadrotor with a flexible cable-suspended payload where cable length and payload mass may vary. Although their configurations and observations differ, both admit the same control structure and can be handled within a unified learning-based framework.

Our primary model is the quadrotor–payload system, which reduces to the quadrotor-only case as $m_P \rightarrow 0$ and the cable constraint becomes inactive. With a taut, massless

cable, the system has eight degrees of freedom, configuration space $SE(3) \times S^2$, and four degrees of underactuation. The dynamics are:

$$\mathbf{x}_Q = \mathbf{x}_P - l \mathbf{q}, \quad (1)$$

$$\dot{\mathbf{x}}_P = \mathbf{v}_P, \quad (2)$$

$$(m_Q + m_P)(\dot{\mathbf{v}}_P + g \mathbf{e}_3) = (\mathbf{q} \cdot f \mathbf{R} \mathbf{e}_3 - m_Q l (\dot{\mathbf{q}} \cdot \dot{\mathbf{q}})) \mathbf{q} + \mathbf{w}_F, \quad (3)$$

$$\dot{\mathbf{q}} = \boldsymbol{\omega} \times \mathbf{q}, \quad (4)$$

$$m_Q l \dot{\boldsymbol{\omega}} = -\mathbf{q} \times f \mathbf{R} \mathbf{e}_3, \quad (5)$$

$$\dot{\mathbf{R}} = \mathbf{R} \dot{\boldsymbol{\Omega}}, \quad (6)$$

$$\mathbf{J}_Q \dot{\boldsymbol{\Omega}} + \boldsymbol{\Omega} \times \mathbf{J}_Q \boldsymbol{\Omega} = \mathbf{M} + \mathbf{w}_M. \quad (7)$$

Here \mathbf{x}_Q and \mathbf{x}_P are the quadrotor and payload positions; m_Q, m_P their masses; $\mathbf{q} \in S^2$ the cable direction; l the cable length; $\mathbf{R} \in SO(3)$ the attitude; f the total thrust; \mathbf{M} the control moment; and $\mathbf{w}_F, \mathbf{w}_M$ external disturbances. Table II summarizes the notation.

This formulation captures the coupled translation–rotation behavior and the nonlinear coupling between thrust direction and payload swing. Removing the payload yields a standard $SE(3)$ quadrotor model; the same RL-learned feedback law applies with a reduced observation space. Using this generalized model, we aim to learn a single policy that robustly tracks reference trajectories across configurations without redesigning model-specific controllers.

B. Arbitrary Trajectory Tracking

We pose a robust reference–tracking problem under dynamic and uncertain conditions. The reference $\mathbf{x}_{\text{ref}}(t)$ is sampled from a family of sinusoid-sum trajectories with randomized amplitudes, frequencies, and phases, and includes hovering intervals at the start and end.

Trained on this distribution, the controller shows zero-shot generalization to unseen references from the same family. The task contains sharp turns and dynamically infeasible segments, where flatness-based geometric controllers typically fail due to the need for precomputed flat outputs.

Robustness is evaluated via:

- **External disturbances:** impulse forces in $[-0.5, 0.5]$ N and torques in $[-0.005, 0.005]$ N·m applied for $[0, 0.5]$ s during hover.
- **Initial-state perturbations:** random offsets in position, orientation, and linear/angular velocity for both quadrotor and payload.

Across cases, the controller rejects disturbances, stabilizes to hover, and resumes accurate tracking, serving as a robust feedback tracker for both system configurations.

IV. END-TO-END MODEL-FREE RL FOR QUADROTOR PAYLOAD TRAJECTORY TRACKING

A. Preliminaries

We formulate the problem as a POMDP \mathcal{M} , defined as a tuple $(\mathcal{S}, \mathcal{A}, \mathcal{O}, \mathcal{T}, \gamma, r)$, where an agent interacts with an environment with state space \mathcal{S} and action space \mathcal{A} , governed by the transition function $\mathcal{T}(\mathbf{s}_{t+1}|\mathbf{s}_t, \mathbf{a}_t)$. The agent

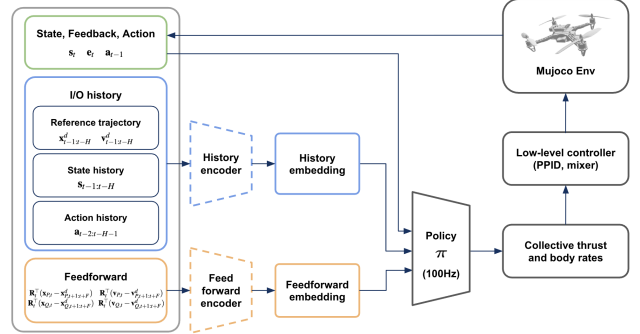


Fig. 1: Block diagram of the policy and training loop. Present features are concatenated with history/preview embeddings and fed to π . CTBR commands pass through the rate loop and mixer before actuation in MuJoCo.

receives an observation $\mathbf{o}_t \in \mathcal{O}$ through the observation function $O(\mathbf{o}_t | \mathbf{s}_t, \mathbf{a}_{t-1})$, which depends on the current state and the previous action. Episodes start from an initial-state distribution ρ_0 over \mathcal{S} , i.e., $\mathbf{s}_0 \sim \rho_0$. Given a reward function $r(\mathbf{o}_t, \mathbf{a}_t)$ and a discount factor γ , the objective in reinforcement learning is to maximize the expected discounted return: $\mathbb{E}[\sum_{t=0}^{\infty} \gamma^t r(\mathbf{o}_t, \mathbf{a}_t)]$. The goal is to learn an optimal policy $\pi^* \in \Pi$ that maps observations $\mathbf{o}_t \in \mathcal{O}$ to optimal actions $\mathbf{a}_t^* \in \mathcal{A}$.

B. Algorithm and Training Overview

We train a policy π_θ that maps observations to actions at 100 Hz. The observation comprises *present*, *past*, and *future* parts: present features $(\mathbf{s}_t, \mathbf{e}_t, \mathbf{a}_{t-1})$; a short I/O history ζ_t of recent states, references, and actions over the last H steps; and a feedforward term ξ_t with previewed position/velocity in the body frame. As in Fig. 1, the history and feedforward stacks pass through optional MLP encoders to form embeddings, which are concatenated with the present features and fed to π_θ . The actor and critic are separate two-layer MLPs (256×256) with SiLU activations. The policy is trained with PPO in a MuJoCo environment [25], [26].

C. State, Action, and Observation Spaces

- 1) **State:** We define the state as

$$\mathbf{s}_t = \begin{bmatrix} \mathbf{x}_{Q,t} & \mathbf{R}_t & \mathbf{x}_{P,t} & \mathbf{v}_{Q,t} \\ \boldsymbol{\omega}_{Q,t} & \mathbf{v}_{P,t} & m_P & l \end{bmatrix}. \quad (8)$$

Position and velocity vectors are normalized element-wise by their respective maxima $x_Q^{\max}, x_P^{\max}, v_Q^{\max}$, and v_P^{\max} . Attitude is represented by a rotation matrix to avoid singularities and remain compatible with geometric-control formulations.

2) **Action:** We adopt a collective thrust and body rates (CTBR) parameterization and convert it to individual rotor thrusts via an inner rate loop and a static mixer [27]. At time t , the policy outputs a normalized action $\mathbf{a}_t = [a_{c,t} \ a_{p,t} \ a_{q,t} \ a_{r,t}] \in [-1, 1]^4$, which we map to the total thrust and desired body-rate setpoints as

$$f_t = \frac{\bar{f}}{2}(1 + a_{c,t}), \quad \boldsymbol{\Omega}_t^d = \bar{\Omega} [a_{p,t} \ a_{q,t} \ a_{r,t}]. \quad (9)$$

A smooth squashing (e.g., tanh) may be used; in practice we use linear rate scaling and an affine map for f_t . The desired rates Ω_t^d are tracked by a per-axis PPID acting on Ω_t with anti-windup and saturation, yielding $\mathbf{M}_t \in \mathbb{R}^3$; this inner loop decouples attitude from thrust and is robust to delays and model mismatch. Finally, (f_t, \mathbf{M}_t) is mapped to single-rotor thrusts via a fixed mixer $\mathbf{A} \in \mathbb{R}^{4 \times 4}$ set by geometry and rotor coefficients,

$$\mathbf{f}_t = \text{clip}(\mathbf{A} [f_t, \mathbf{M}_t], 0, \bar{f}), \quad (10)$$

and, in simulation, passed through first-order motor dynamics. To reduce sim-to-real gap, we also inject a 10–30 ms discrete input delay at 100 Hz and apply a first-order rotor lag with asymmetric rise/fall time constants, randomized during training.

3) *Observation*: The observation captures the current state, short I/O history, and a preview of the reference, providing context for robust decisions. It is structured as

$$\mathbf{o}_t = [\mathbf{s}_t \quad \mathbf{e}_t \quad \mathbf{a}_{t-1} \quad \zeta_t \quad \xi_t], \quad (11)$$

where \mathbf{s}_t is the current state and \mathbf{a}_{t-1} the previous action.

$\mathbf{e}_t \in \mathbb{R}^{12}$ is the body-frame tracking error:

$$\mathbf{e}_t = [\mathbf{R}_t^\top \mathbf{e}_{x_{P,t}} \quad \mathbf{R}_t^\top \mathbf{e}_{v_{P,t}} \quad \mathbf{R}_t^\top \mathbf{e}_{x_{Q,t}} \quad \mathbf{R}_t^\top \mathbf{e}_{v_{Q,t}}], \quad (12)$$

where $\mathbf{e}_{x_P}, \mathbf{e}_{v_P}, \mathbf{e}_{x_Q}, \mathbf{e}_{v_Q}$ are the position/velocity errors for payload and quadrotor.

ζ_t is the I/O history:

$$\zeta_t = [\mathbf{s}_{t-1:t-H} \quad \mathbf{x}_{t-1:t-H}^d \quad \mathbf{v}_{t-1:t-H}^d \quad \mathbf{a}_{t-2:t-H-1}], \quad (13)$$

with buffer length $H=5$ and

$$\begin{aligned} \mathbf{x}_{t-1:t-H}^d &= [\mathbf{x}_{Q,t-1:t-H}^d \quad \mathbf{x}_{P,t-1:t-H}^d], \\ \mathbf{v}_{t-1:t-H}^d &= [\mathbf{v}_{Q,t-1:t-H}^d \quad \mathbf{v}_{P,t-1:t-H}^d]. \end{aligned} \quad (14)$$

ξ_t is the body-frame feedforward term w.r.t. the previewed reference:

$$\xi_t = \begin{bmatrix} \mathbf{R}_t^\top (\mathbf{x}_{P,t} - \mathbf{x}_{P,t+1:t+F}^d) & \mathbf{R}_t^\top (\mathbf{v}_{P,t} - \mathbf{v}_{P,t+1:t+F}^d) \\ \mathbf{R}_t^\top (\mathbf{x}_{Q,t} - \mathbf{x}_{Q,t+1:t+F}^d) & \mathbf{R}_t^\top (\mathbf{v}_{Q,t} - \mathbf{v}_{Q,t+1:t+F}^d) \end{bmatrix} \quad (15)$$

To emulate sensor imperfections and promote robustness under partial observability, we inject clipped Gaussian noise during training: positions $\mathbf{x}_Q, \mathbf{x}_P$ use $\sigma_x=0.01$ m with ± 2.5 mm clipping; linear velocities $\mathbf{v}_Q, \mathbf{v}_P$ use $\sigma_v=0.02$ m/s with ± 5 mm/s clipping; attitude uses $\mathbf{R} = \mathbf{R}(\theta + \eta_\theta)$ with $\sigma_\theta=\pi/60$ rad and $\pm\pi/120$ rad clipping; body rates Ω use $\sigma_\Omega=\pi/30$ rad/s with $\pm\pi/60$ rad/s clipping.

In principle, a full history would be ideal but is intractable; a fixed-length buffer offers a practical POMDP approximation that preserves essential temporal information [28]. While I/O history is common in legged locomotion [29], [30], high control rates in aerial robots (often > 50 Hz) make compact encodings important. With a payload, the hybrid and more underactuated dynamics further increase the value of history: it aids implicit dynamics learning (analogous to model-based RL that first learns dynamics, then optimizes control [31]) and provides temporal feedback that improves robustness

to delays and sensor noise [29]. Finally, organizing the observation into *present* (feedback/state/action), *past* (I/O history), and *future* (feedforward preview) mirrors finite-horizon optimal-control structure (e.g., MPC) and helps the policy exploit known future references when maximizing return [32].

D. Rewards and Episode Design

1) *Reward structure*: We balance tracking accuracy with stable, smooth control by summing exponentiated penalties on key quantities (position, yaw, body rates, cable motion, action magnitude, and action variation):

$$\begin{aligned} r_{x_P} &= w_{x_P} \exp(-\alpha_{x_P} \|\mathbf{x}_{P,t} - \mathbf{x}_{P,t}^d\|), \\ r_\psi &= w_\psi \exp(-\alpha_\psi |\psi_t|), \\ r_\Omega &= w_\Omega \exp(-\alpha_\Omega \|\Omega_t\|), \\ r_{\dot{q}} &= w_{\dot{q}} \exp(-\alpha_{\dot{q}} \|\dot{\mathbf{q}}_t\|), \\ r_a &= w_a \exp(-\alpha_a \|\mathbf{a}_t\|), \\ r_{\Delta a} &= w_{\Delta a} \exp(-\alpha_{\Delta a} \|\Delta \mathbf{a}_t\|). \end{aligned} \quad (16)$$

Here ψ_t is the yaw angle, $\dot{\mathbf{q}}_t$ is the rate of the cable direction (approximated via relative quadrotor–payload velocity normalized by cable length), $\Delta \mathbf{a}_t$ is an exponentially weighted L_2 norm of recent action changes, and α_k, w_k are scale and weight coefficients. The total reward is

$$r_t = r_{x_P} (1 + r_\psi + r_\Omega + r_{\dot{q}}) + r_a + r_{\Delta a}. \quad (17)$$

This structure prioritizes accurate payload tracking and further rewards low yaw, low body rates, and small cable motion, while discouraging large or rapidly changing actions.

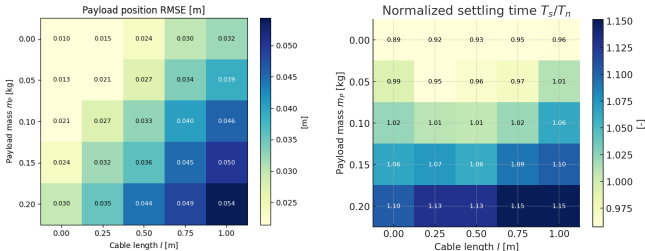
2) *Early termination*: For sample efficiency, episodes terminate on failure: ground contact ($z_Q < 0$), excessive payload error $\|\mathbf{x}_{P,t} - \mathbf{x}_{P,t}^d\| > \varepsilon_{\text{pos}}$ or $\|\mathbf{v}_{P,t} - \mathbf{v}_{P,t}^d\| > \varepsilon_{\text{vel}}$, or if any quadrotor Euler angle exceeds $\pi/2$ in magnitude.

E. Control Perspective and Stability Considerations

At a high level, the learned policy issues CTBR commands while a faster rate-PPID and static mixer produce body moments and single-rotor thrusts; with anti-windup and saturation, the inner loop behaves nearly as an identity from Ω^d to body rates.

Robustness view. Around hover, the inner loop stabilizes the rotation while the outer loop acts on the translational/cable dynamics through thrust direction and magnitude. With bounded delays and first-order rotor lags, a small-gain/ISS argument implies bounded tracking error provided: (i) the rate loop remains stable with margin under saturation; (ii) the policy outputs are bounded (by design); and (iii) disturbances enter as additive inputs. Domain randomization effectively enlarges these margins by training across variability in (m_P, l) and aerodynamics.

Energy/damping view. The reward terms on body rates and cable motion ($r_\Omega, r_{\dot{q}}$) act as damping injection for the coupled quadrotor–pendulum modes, while CTBR allows smooth thrust–direction shaping. This encourages thrust alignment with the cable tension and attenuates swing without an explicit model.



(a) Payload position RMSE. (b) Normalized settling time T_s/T_n .

Fig. 2: Zero-shot performance across payload mass m_P and cable length l on unseen trajectories.

F. Domain Randomization

To promote robustness and generalization, we apply domain randomization at the start of each training episode [33]. For the quadrotor, we perturb body mass, inertia, center of mass, and the orientation of the local inertia frame (via randomized translations and quaternion rotations); actuator inconsistencies are modeled by varying motor gear coefficients. For the suspended payload, mass and cable length are uniformly sampled from $[0.0, 0.2]$ kg and $[0.0, 1.0]$ m, respectively, and the payload pose and cable constraints are updated accordingly. We also randomize near-ground aerodynamic effects: when $z < 0.5$ m, a force with direction sampled from the upper hemisphere is applied, with magnitude increasing as altitude decreases. Jointly randomizing these physical and aerodynamic properties exposes the policy to cases ranging from no payload to strong disturbances, yielding zero-shot generalization without controller switching or environment-specific tuning. Empirical performance across the randomized configuration grid is summarized in the heatmaps of Fig. 2.

G. Belief-Based Analysis of I/O History in Partially Observable Hybrid Systems

In partially observable systems such as the quadrotor-payload system, inferring the full state \mathbf{s}_t from a single observation \mathbf{o}_t is intractable due to hybrid dynamics from the flexible cable. We therefore use a fixed-length history of observations and actions (*I/O history*) to approximate the belief state and briefly justify this choice.

1) *Belief-Based Policy and Value under Uncertainty*: In partially observable settings, the agent maintains a belief over the latent state, updated via Bayesian filtering:

$$b_t(\mathbf{s}_t) = p(\mathbf{s}_t \mid \mathbf{o}_{0:t}, \mathbf{a}_{0:t-1}) \\ = \frac{O(\mathbf{o}_t \mid \mathbf{s}_t, \mathbf{a}_{t-1})}{p(\mathbf{o}_t \mid \mathbf{o}_{0:t-1}, \mathbf{a}_{0:t-1})} \sum_{\mathbf{s}_{t-1}} T(\mathbf{s}_t \mid \mathbf{s}_{t-1}, \mathbf{a}_{t-1}) b_{t-1}(\mathbf{s}_{t-1}) \quad (18)$$

This update reduces entropy by exploiting temporal context:

$$H(\mathbf{s}_t \mid \mathbf{o}_{0:t}, \mathbf{a}_{0:t-1}) \leq H(\mathbf{s}_t \mid \mathbf{o}_t). \quad (19)$$

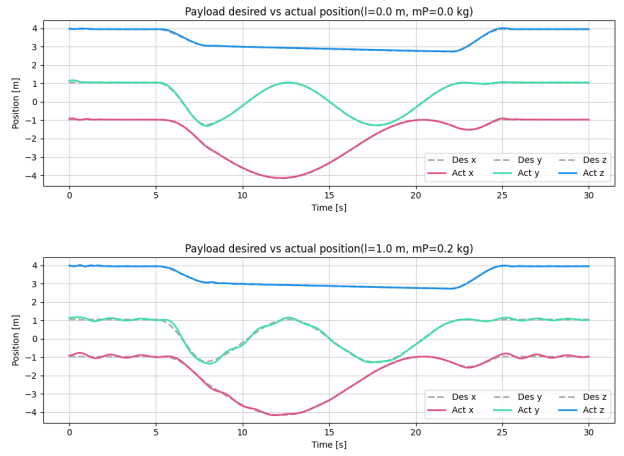


Fig. 3: Payload tracking on unseen trajectories: without payload (top) and with flexible cable-suspended payload (bottom).

Lower-entropy beliefs improve performance under the value function:

$$V^*(b_t) = \max_{\mathbf{a}_t} \left[\sum_{\mathbf{s}_t} b_t(\mathbf{s}_t) R(\mathbf{s}_t, \mathbf{a}_t) + \gamma \sum_{\mathbf{o}_{t+1}} p(\mathbf{o}_{t+1} \mid b_t, \mathbf{a}_t) V^*(b_{t+1}) \right], \quad (20)$$

and satisfy $V^*(b_t) \geq V^*(b'_t)$ for any less informative belief $b'_t(\mathbf{s}_t) = p(\mathbf{s}_t \mid \mathbf{o}_t)$. In actor-critic terms, concentrated beliefs yield sharper value estimates:

$$b_t(\mathbf{s}_t) \approx \delta(\mathbf{s}_t - \mathbf{s}_t^*) \Rightarrow V^\pi(b_t) \approx \sum_{\mathbf{a}_t} \pi(\mathbf{a}_t \mid b_t) Q^\pi(\mathbf{s}_t^*, \mathbf{a}_t), \quad (21)$$

$$b_t(\mathbf{s}_t) \approx \mathcal{U}(S) \Rightarrow V^\pi(b_t) \approx \frac{1}{|\mathcal{S}|} \sum_{\mathbf{s}_t, \mathbf{a}_t} \pi(\mathbf{a}_t \mid b_t) Q^\pi(\mathbf{s}_t, \mathbf{a}_t). \quad (22)$$

Hence, belief accuracy is critical in POMDPs.

2) *Hybrid Dynamics and Mode Estimation*: Flexible cables induce hybrid dynamics:

$$\Sigma = \begin{cases} \mathbf{s}_{t+1} = f_m(\mathbf{s}_t, \mathbf{a}_t), & m \in \{\text{taut, slack}\}, \\ \mathbf{s}_{t+1}^+ = \Delta_{m^- \rightarrow m^+}(\mathbf{s}_t^-), & \mathbf{s}_t \in S_{\text{switch}}, \end{cases} \quad (23)$$

where the mode m_t is unobserved. The agent maintains a joint belief over mode and state:

$$b_t(m_t, \mathbf{s}_t) = p(m_t, \mathbf{s}_t \mid \mathbf{o}_{0:t}, \mathbf{a}_{0:t-1}). \quad (24)$$

Updating the mode belief marginalizes past modes and states:

$$p(m_t \mid \mathbf{o}_{0:t}, \mathbf{a}_{0:t-1}) \propto \sum_{m_{t-1}} \int p(m_t \mid m_{t-1}, \mathbf{s}_{t-1}, \mathbf{a}_{t-1}) \\ \times b_{t-1}(m_{t-1}, \mathbf{s}_{t-1}) d\mathbf{s}_{t-1}. \quad (25)$$

Because mode transitions depend on latent variables, a single observation \mathbf{o}_t is insufficient; temporal context is needed to disambiguate modes. Entropy shrinks with longer histories:

$$H(m_t, \mathbf{s}_t \mid \mathbf{o}_t) > H(m_t, \mathbf{s}_t \mid \mathbf{o}_{t-1}, \mathbf{o}_t, \mathbf{a}_{t-1}) \\ > H(m_t, \mathbf{s}_t \mid \mathbf{o}_{0:t}, \mathbf{a}_{0:t-1}). \quad (26)$$

Parameters	Values
Mass	0.280 kg
Inertia around x, y	$2.36 \times 10^{-4} \text{ kg} \cdot \text{m}^2$
Inertia around z	$3.03 \times 10^{-4} \text{ kg} \cdot \text{m}^2$
Arm Length	0.058 m
Propeller Thrust Factor	$1.145 \times 10^{-7} \text{ N} \cdot \text{s}^2$
Payload Mass	0.025 kg

TABLE III: Quadrotor parameters.

Thus, I/O history is essential for reducing uncertainty over both mode and state, and is particularly beneficial for robust control in quadrotor–payload systems with hybrid, stochastic dynamics—as corroborated by the ablation results in Table IV.

V. EXPERIMENTS

We evaluate ROVERFLY on trajectory tracking and hover stabilization in both *quadrotor-only* and *flexible cable–suspended payload* configurations. Unless noted otherwise, a *single* end-to-end policy (no controller switching or re-tuning) is used for all conditions. The policy runs at 100 Hz and the simulator at 500 Hz. During training we inject sensor noise, an actuation delay of 10–30 ms, and parameter randomization. Quadrotor parameters are summarized in Table III.

A. Tasks and Evaluation Protocol

We consider two tasks: (i) **arbitrary trajectory tracking** under unseen references and disturbances, and (ii) **hover stabilization** under large initial perturbations. For tracking, reference families are generated by summing sinusoids with randomized amplitudes, frequencies, and phases; evaluation uses held-out trajectories (zero-shot). For hover, we apply a randomized initial state perturbation and measure recovery.

For tracking, we report per-axis position RMSE and the time-averaged RMSE norm. For hover, we use the settling-time metric $T_s = \min\{t : |e(\xi)| \leq \varepsilon, \forall \xi \in [t, t + \tau]\}$, with $\varepsilon = 0.01$ m and $\tau = 0.5$ s, the normalized T_s/T_n with $T_n = 2\pi\sqrt{l/g}$ (cable–pendulum natural period), and the steady-state error e_{ss} computed as the mean error over the last 0.5 s. All results aggregate multiple random seeds and unseen trajectories.

B. Zero-Shot Tracking Across Payload Configurations

We evaluate the same policy at two endpoints of the domain: *without payload* ($l=0.0$ m, $m_P=0.0$ kg) and *with flexible payload* ($l=1.0$ m, $m_P=0.2$ kg). The controller tracks the desired payload CoM in x, y, z without any controller switching. Quantitatively, without a payload the RMSE is $x = 0.008$ m, $y = 0.010$ m, $z = 0.008$ m (total 0.016 m); with a flexible cable-suspended payload it is $x = 0.024$ m, $y = 0.010$ m, $z = 0.006$ m (total 0.034 m). The policy remains stable through hover segments and aggressive turns, illustrating strong zero-shot generalization across dynamics.

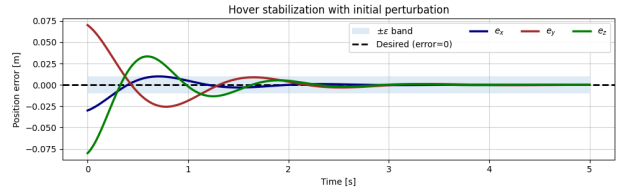


Fig. 4: Hover initial perturbation rejection: position error traces ($l=1.0$ m, $m_P=0.2$ kg).

C. Hover Stabilization and Disturbance Rejection

For hover, we sample an initial perturbation as $\Delta\mathbf{x}_Q \sim \mathcal{U}([-0.1, 0.1]^3)$ m applied to both quadrotor and payload positions, $\Delta\mathbf{v}_Q \sim \mathcal{U}([-0.1, 0.1]^3)$ m/s to both linear velocities, $\Delta\theta_Q \sim \mathcal{U}(-\pi/12, \pi/12]^3)$ rad to the quadrotor attitude, and $\Delta\Omega \sim \mathcal{U}(-\pi/12, \pi/12]^3)$ rad/s to the quadrotor body rates. The payload error responses (e_x, e_y, e_z) remain within a small neighborhood and converge with $e_{ss} \approx 0$. For $l=1.0$ m, the observed settling time is on the order of a single natural period ($T_n \approx 2.0$ s), indicating physically consistent recovery under underactuated cable–pendulum dynamics.

D. Generalization Over Payload Mass and Cable Length

We assess zero-shot generalization over a grid $m_P \in [0, 0.2]$ kg and $l \in [0, 1]$ m using unseen trajectories and multiple seeds per cell. Figure 2 reports payload-position RMSE (tracking accuracy) and normalized settling time T_s/T_n (recovery speed relative to T_n). RMSE grows with heavier payloads and longer cables, reflecting increased inertia and underactuation rather than brittle failures. Most T_s/T_n values lie near 1–1.3, indicating recovery within about one natural period. Short cables ($l \approx 0$) yield the fastest recovery and smallest errors; larger l introduces more oscillation yet remains well damped. Increasing m_P slows the response but does not destabilize the policy. These trends indicate that domain/task randomization together with the history- and feedforward-augmented observation support a single policy that generalizes across (m_P, l) without task-specific design or re-tuning.

E. Ablation on I/O History

We quantify the effect of temporal context (the last H steps of state/action/reference). Using the same trained policy and evaluation setup, we vary $H \in \{0, 1, 5, 10\}$ on unseen trajectories for two configurations: no payload ($l=0$, $m_P=0$) and a flexible payload ($l=1.0$ m, $m_P=0.2$ kg). Table IV reports payload position RMSE (per-axis and total).

Temporal history helps in both cases but is markedly more important with a flexible cable: removing history increases total RMSE from 0.054 to 0.075 (+40%) with payload, versus 0.010 to 0.021 (+110%) without payload. A minimal buffer ($H=1$) recovers part of the loss, a short window ($H=5$) is near-optimal under hybrid (taut/slack) dynamics and delay, and $H=10$ gives only marginal gains.

TABLE IV: Effect of I/O history length H on payload position RMSE (m) for unseen trajectories.

Configuration	H	RMSE $_x$	RMSE $_y$	RMSE $_z$	Total
$l=0, m_P=0$	0	0.011	0.014	0.010	0.021
	1	0.010	0.012	0.009	0.018
	5	0.008	0.010	0.008	0.016
	10	0.007	0.006	0.003	0.010
$l=1.0, m_P=0.2$	0	0.051	0.047	0.031	0.075
	1	0.049	0.043	0.029	0.072
	5	0.045	0.041	0.025	0.066
	10	0.038	0.032	0.020	0.054

F. Reference Trajectory Generation

We generate a family of *payload-centric* references that combine (i) explicit hover segments and (ii) smooth oscillatory motion with randomized amplitudes and frequencies. Each episode draws

$$(a_x, a_y) \sim \mathcal{U}([-2, 2]), a_z \sim \mathcal{U}([-1, 1]), \quad (27)$$

$$(f_1, f_2) \sim \mathcal{U}([-0.2, 0.2]), f_3 \sim \mathcal{U}([-0.1, 0.1]). \quad (28)$$

with fixed phases $\phi_x, \phi_y, \phi_z \in \{\frac{\pi}{2}, \frac{3\pi}{2}\}$. Let $\omega_i = 2\pi f_i$ and t_f be the episode horizon. Hover at the beginning and end is enforced by a smooth window $w(t) \in [0, 1]$:

$$w(t) = \begin{cases} 0, & t < t_s \text{ or } t > t_e, \\ 3\alpha^2 - 2\alpha^3, & t \in [t_s, t_s + \Delta], \alpha = \frac{t - t_s}{\Delta}, \\ 1, & t \in [t_s + \Delta, t_e - \Delta], \\ 3\beta^2 - 2\beta^3, & t \in [t_e - \Delta, t_e], \beta = \frac{t_e - t}{\Delta}, \end{cases} \quad (29)$$

with $t_s = 5$ s, $t_e = t_f - 5$ s, and transition duration $\Delta = 3$ s. Its derivative $\dot{w}(t)$ avoids velocity/acceleration discontinuities at the transitions.

1) *Payload reference*: The desired payload position, velocity, and acceleration are

$$\begin{aligned} \mathbf{x}_P^d(t) &= \begin{bmatrix} w(t) A_x (1 - \cos(\omega_1 t + \phi_x)) \\ w(t) A_y (1 - \cos(\omega_2 t + \phi_y)) \\ w(t) A_z (1 - \cos(\omega_3 t + \phi_z)) \end{bmatrix}, \\ \mathbf{v}_P^d(t) &= \dot{\mathbf{x}}_P^d(t), \quad \mathbf{a}_P^d(t) = \ddot{\mathbf{x}}_P^d(t). \end{aligned} \quad (30)$$

We cap nominal peak speed by normalizing (A_x, A_y, A_z) if $\max\{A_x|\omega_1|, A_y|\omega_2|, A_z|\omega_3|\} > v_{\max}$ with $v_{\max} = 4$ m/s, ensuring comparable difficulty across draws while still covering aggressive segments.

2) *Cable direction and quadrotor reference*: Given payload mass m_P and gravity $\mathbf{g} = g\mathbf{e}_3$, define

$$\mathbf{T}_P(t) = -m_P(\mathbf{a}_P^d(t) + \mathbf{g}), \quad \mathbf{q}^d(t) = \frac{\mathbf{T}_P(t)}{\|\mathbf{T}_P(t)\|}. \quad (31)$$

We obtain $\dot{\mathbf{q}}^d$ and $\ddot{\mathbf{q}}^d$ by differentiating \mathbf{T}_P . For cable length l , the quadrotor position reference is

$$\mathbf{x}_Q^d(t) = \mathbf{x}_P^d(t) - l \mathbf{q}^d(t), \quad (32)$$

with velocities/accelerations derived analogously.

This design (i) enforces hover at the start/end for consistent stabilization evaluation, (ii) excites

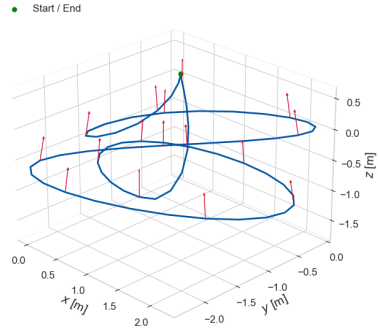


Fig. 5: Example payload trajectory with nominal cable-tension directions (red).

coupled translation–pendulum modes via randomized amplitudes/frequencies, and (iii) preserves smooth motion on/off through $w(t)$ and $\dot{w}(t)$. Randomization over $(A_x, A_y, A_z, f_1, f_2, f_3)$ yields a controlled yet diverse task distribution; zero-shot tests use held-out parameters and unseen trajectories from the same family to probe robustness across payload mass, cable length, and reference complexity.

VI. CONCLUSION AND FUTURE WORK

We presented ROVERFLY, a unified learning-based controller that tracks arbitrary trajectories and stabilizes from disturbances across payload conditions, from no payload to flexible cable–suspended loads with varying mass and cable length. A single policy, trained with task and domain randomization, handles changes in (m_P, l) without controller switching or re-tuning. The observation design combines present feedback, short I/O history, and finite-horizon feed-forward terms, and the CTBR action parameterization yields smooth attitude shaping and effective payload damping.

Experiments show (i) low tracking error across configurations, (ii) rapid disturbance rejection with near-zero steady-state error and settling times on the order of one pendulum period, (iii) smooth performance trends over (m_P, l) without brittle failures, and (iv) ablations confirming the value of history and feedforward information. Together, these results indicate strong zero-shot generalization of a *single* policy across hybrid, underactuated regimes.

Limitations. We assume a taut, massless cable; slack–taut transitions and contact events are only partially captured. Evaluation is in high-fidelity simulation; real-world sensing artifacts, unmodeled aerodynamics, and onboard compute limits are not yet systematically assessed. Finally, the deployed policy has no formal safety or constraint guarantees.

Future work. We will (i) validate on hardware across platforms and sensors, including vision-in-the-loop estimation; (ii) extend coverage to slack cables, contact, and time-varying cable length, and benchmark under aggressive, dynamically infeasible references; (iii) integrate safety wrappers (e.g., control-barrier-function shields) and online identification of (m_P, l) for constraint-aware adaptation; (iv) explore meta-RL and few-shot test-time adaptation for out-

of-distribution payloads and environments; (v) scale to multi-UAV cooperative transport and manipulation; and (vi) develop analytical links (e.g., input-to-state stability, robustness margins) between the learned policy and classical control guarantees.

REFERENCES

- [1] T. Lee, M. Leok, and N. H. McClamroch, “Geometric tracking control of a quadrotor uav on se (3),” in *49th IEEE conference on decision and control (CDC)*, IEEE, 2010, pp. 5420–5425.
- [2] E. Kaufmann, L. Bauersfeld, A. Loquercio, M. Müller, V. Koltun, and D. Scaramuzza, “Champion-level drone racing using deep reinforcement learning,” *Nature*, vol. 620, no. 7976, pp. 982–987, 2023.
- [3] J. Thomas, J. Polin, K. Sreenath, and V. Kumar, “Avian-inspired grasping for quadrotor micro uavs,” in *International Design Engineering Technical Conferences and Computers and Information in Engineering Conference*, American Society of Mechanical Engineers, vol. 55935, 2013, V06AT07A014.
- [4] K. Sreenath, T. Lee, and V. Kumar, “Geometric control and differential flatness of a quadrotor uav with a cable-suspended load,” in *52nd IEEE Conference on Decision and Control*, 2013, pp. 2269–2274. DOI: 10.1109/CDC.2013.6760219
- [5] T. Lee, K. Sreenath, and V. Kumar, “Geometric control of cooperating multiple quadrotor uavs with a suspended payload,” in *52nd IEEE Conference on Decision and Control*, 2013, pp. 5510–5515. DOI: 10.1109/CDC.2013.6760757
- [6] S. Tang and V. Kumar, “Mixed integer quadratic program trajectory generation for a quadrotor with a cable-suspended payload,” in *2015 IEEE International Conference on Robotics and Automation (ICRA)*, 2015, pp. 2216–2222. DOI: 10.1109/ICRA.2015.7139492
- [7] S. Tang, K. Sreenath, and V. Kumar, “Multi-robot trajectory generation for an aerial payload transport system,” in *Robotics Research*, N. M. Amato, G. Hager, S. Thomas, and M. Torres-Torriti, Eds., Cham: Springer International Publishing, 2020, pp. 1055–1071.
- [8] P. Foehn, D. Falanga, N. Kuppuswamy, R. Tedrake, and D. Scaramuzza, “Fast trajectory optimization for agile quadrotor maneuvers with a cable-suspended payload,” 2017.
- [9] P. Kotaru, G. Wu, and K. Sreenath, “Dynamics and control of a quadrotor with a payload suspended through an elastic cable,” in *2017 American Control Conference (ACC)*, 2017, pp. 3906–3913. DOI: 10.23919/ACC.2017.7963553
- [10] P. Kotaru, G. Wu, and K. Sreenath, “Differential-flatness and control of quadrotor(s) with a payload suspended through flexible cable(s),” in *2018 Indian Control Conference (ICC)*, 2018, pp. 352–357. DOI: 10.1109/INDIANCC.2018.8308004
- [11] J. Zeng, P. Kotaru, and K. Sreenath, “Geometric control and differential flatness of a quadrotor uav with load suspended from a pulley,” in *2019 American Control Conference (ACC)*, 2019, pp. 2420–2427. DOI: 10.23919/ACC.2019.8815173
- [12] J. Zeng, P. Kotaru, M. W. Mueller, and K. Sreenath, “Differential flatness based path planning with direct collocation on hybrid modes for a quadrotor with a cable-suspended payload,” *IEEE Robotics and Automation Letters*, vol. 5, no. 2, pp. 3074–3081, 2020. DOI: 10.1109/LRA.2020.2972845
- [13] T. Lee, “Geometric control of quadrotor uavs transporting a cable-suspended rigid body,” *IEEE Transactions on Control Systems Technology*, vol. 26, no. 1, pp. 255–264, 2018. DOI: 10.1109/TCST.2017.2656060
- [14] J. Hwangbo, I. Sa, R. Siegwart, and M. Hutter, “Control of a quadrotor with reinforcement learning,” *IEEE Robotics and Automation Letters*, vol. 2, no. 4, pp. 2096–2103, 2017. DOI: 10.1109/LRA.2017.2720851
- [15] K. Huang, R. Rana, A. Spitzer, G. Shi, and B. Boots, “Datt: Deep adaptive trajectory tracking for quadrotor control,” *arXiv preprint arXiv:2310.09053*, 2023.
- [16] J. Cai, V. Sangli, M. Kim, and K. Sreenath, “Learning-based trajectory tracking for bird-inspired flapping-wing robots,” *arXiv preprint arXiv:2411.15130*, 2024. DOI: 10.48550/arXiv.2411.15130
- [17] L. Bauersfeld, K. Müller, D. Ziegler, F. Coletti, and D. Scaramuzza, “Robotics meets fluid dynamics: A characterization of the induced airflow below a quadrotor as a turbulent jet,” *IEEE Robotics and Automation Letters*, 2024.
- [18] B. Gupta, M. Kim, A. Park, E. Sihite, K. Sreenath, and A. Ramezani, “Estimation of aerodynamics forces in dynamic morphing wing flight,” *arXiv preprint arXiv:2508.02984*, 2025. DOI: 10.48550/arXiv.2508.02984
- [19] E. Kaufmann, A. Loquercio, R. Ranftl, M. Müller, V. Koltun, and D. Scaramuzza, “Deep drone acrobatics,” *arXiv preprint arXiv:2006.05768*, 2020.
- [20] D. Zhang, A. Loquercio, X. Wu, A. Kumar, J. Malik, and M. W. Mueller, “Learning a single near-hover position controller for vastly different quadcopters,” in *2023 IEEE International Conference on Robotics and Automation (ICRA)*, 2023, pp. 1263–1269. DOI: 10.1109/ICRA48891.2023.10160836
- [21] R. Zhang, D. Zhang, and M. W. Mueller, “Proxfly: Robust control for close proximity quadcopter flight via residual reinforcement learning,” *arXiv preprint arXiv:2409.13193*, 2024.
- [22] B. Xu, F. Gao, C. Yu, R. Zhang, Y. Wu, and Y. Wang, “Omnidrones: An efficient and flexible platform for reinforcement learning in drone control,” *IEEE Robotics and Automation Letters*, vol. 9, no. 3, pp. 2838–2844, 2024. DOI: 10.1109/LRA.2024.3356168
- [23] J. Eschmann, D. Albani, and G. Loianno, “Learning to fly in seconds,” *IEEE Robotics and Automation Letters*, vol. 9, no. 7, pp. 6336–6343, 2024. DOI: 10.1109/LRA.2024.3396025
- [24] S. Belkhale, R. Li, G. Kahn, R. McAllister, R. Calandra, and S. Levine, “Model-based meta-reinforcement learning for flight with suspended payloads,” *IEEE Robotics and Automation Letters*, vol. 6, no. 2, pp. 1471–1478, 2021. DOI: 10.1109/LRA.2021.3057046
- [25] J. Schulman, F. Wolski, P. Dhariwal, A. Radford, and O. Klimov, “Proximal policy optimization algorithms,” *arXiv preprint arXiv:1707.06347*, 2017.
- [26] E. Todorov, T. Erez, and Y. Tassa, “Mujoco: A physics engine for model-based control,” in *2012 IEEE/RSJ international conference on intelligent robots and systems*, IEEE, 2012, pp. 5026–5033.
- [27] E. Kaufmann, L. Bauersfeld, and D. Scaramuzza, “A benchmark comparison of learned control policies for agile quadrotor flight,” in *2022 International Conference on Robotics and Automation (ICRA)*, IEEE, 2022, pp. 10504–10510.
- [28] N. Meuleau, L. Peshkin, K.-E. Kim, and L. P. Kaelbling, “Learning finite-state controllers for partially observable environments,” *arXiv preprint arXiv:1301.6721*, 2013.
- [29] Z. Li, X. B. Peng, P. Abbeel, S. Levine, G. Berseth, and K. Sreenath, “Reinforcement learning for versatile, dynamic, and robust bipedal locomotion control,” *The International Journal of Robotics Research*, vol. 0, no. 0, p. 02783649241285161, 0. DOI: 10.1177/02783649241285161
- [30] X. B. Peng, M. Andrychowicz, W. Zaremba, and P. Abbeel, “Sim-to-real transfer of robotic control with dynamics randomization,” in *2018 IEEE international conference on robotics and automation (ICRA)*, IEEE, 2018, pp. 3803–3810.
- [31] K. Chua, R. Calandra, R. McAllister, and S. Levine, “Deep reinforcement learning in a handful of trials using probabilistic dynamics models,” *Advances in neural information processing systems*, vol. 31, 2018.
- [32] D. Bertsekas, *Dynamic programming and optimal control: Volume I*. Athena scientific, 2012, vol. 4.
- [33] J. Tobin, R. Fong, A. Ray, J. Schneider, W. Zaremba, and P. Abbeel, “Domain randomization for transferring deep neural networks from simulation to the real world,” in *2017 IEEE/RSJ International Conference on Intelligent Robots and Systems (IROS)*, 2017, pp. 23–30. DOI: 10.1109/IROS.2017.8202133